University of Gothenburg

Master of Science Thesis

Optimization of uTE scan protocol for human lung MR imaging

Author: Katrin Johansson

Supervisor: PhD. Kerstin Lagerstrand

DEPARTMENT OF RADIATION PHYSICS, UNIVERSITY OF GOTHENBURG

January 2011

Acknowledgements

I would like to thank my supervisor Kerstin Lagerstrand for all the time, effort and enthusiasm that she has spent on this work. Without her support, this challenge would have been even bigger for me. I would also like to thank the MR physisists and fellow students with whom I have discussed details of this work. My family have been a great support during my entire education. For this I am deeply grateful.

Abstract

Background

Ultra short echo time (uTE) sequences are suitable for imaging of tissues with short T2 or T2* relaxation times, such as lung. The ultra short echo time is possible because of the short excitation pulse, the radial k-space trajectory and gradient ramp sampling.

The aim of this work is to study if the signal behaviour of a non commersial uTE sequence follows theoretically expected associations, and to optimize the sequence with purpose to increase its performance in human lung imaging.

Methods

Two different phantoms were used to study the signal behaviour - including noise, motion disturbance and signal leakage - of the uTE sequence. The signal behaviour of the uTE sequence was compared to the signal behaviour of a corresponding asymmetric gradient echo sequence. *In vivo* lung images were acquired before and after optimization of the uTE scan protocol.

Results

The uTE signal increased with increased radial density and voxel size, and with decreased echo time and bandwidth. Results showed differences in signal behaviour between the uTE sequence and a corresponding asymmetric gradient echo sequence. *In vivo* images showed improvement in visability and resolution after scan protocol optimization.

Conclusion

This work elucidated the signal behaviour of the uTE sequence. Via this knowledge, combined with previous knowledge about well-established theoretical associations, the quality of *in vivo* lung MR images could be improved. Further understanding of the uTE regridding and density weighting process is needed to continue the optimization process.

Contents

List of Figures

1 INTRODUCTION

Ultra short echo time sequences - referred to as uTE sequences - have the potential to image tissues with short T_2 or T_2* relaxation times [1]. The echo time (TE) for a uTE sequence can be as short as 100 μs, which is possible because of the short excitation pulse, the radial k-space trajectory and gradient ramp sampling. Since the readout is radial and starts at the center of k-space, the sampled signal shows the free induction decay. Before image reconstruction, the radial k-space data is regridded to a Cartesian matrix and corrected via a density weighting function for the oversampled radial data [2]. In 3D uTE, the excitation pulse is a very short RF block pulse. The T2* relaxation during excitation is therefore minimized and the effective time point of excitation is towards the end of the pulse.

uTE sequences give rise to special properties that need to be concidered when imaging is performed. The oversampling of data in the middle of k-space will result in enhanced SNR. Also, the appearance of motion and aliasing artefacts is different compared with Cartesian sequences. Aliasing can occur in either the angular or the radial direction, which in the images creates either streakings or object repetition in circles at periodic distances from the image center [3]. Object motion in the direction of the radials results in a motion artefact that is evenly distributed over the image [4]. Finally, all corrections used in uTE imaging (e.g. density weighting and eddy current and gradient ramp sampling compensations) affect the appearance of the object in the image [2].

Some of the properties of the uTE sequence - potentially high SNR for short T_2* tissue and motion insensitivity due to the evenly distributed artifact - make this sequence suitable for lung imaging. In the thorax region there are cardiac and respiratory motion that can create disturbances in the images. The low proton density of the lung parenchyma and the short T2* originating from the large susceptibility differences between air and lung parenchyma give low signal from

the lungs that decays rapidly with T2*. Previous research on uTE in human lung imaging has showed promising results [5] [6]. Research on small rodents has also shown that lung imaging will benefit from using uTE sequences, since it can improve the SNR [7] [8]. The question is, though, if the uTE sequence also adds unwanted signal that does not originate from lung parenchyma.

The aim of this work is to study if the signal behaviour of a non commersial uTE sequence follows theoretically expected associations, and to optimize the sequence with purpose to increase its performance in human lung imaging.

2 MATERIAL AND METHODS

2.1 MRI MEASUREMENTS

Measurements in this work have been performed on a 1.5 T clinical MR scanner (Philips Achieva, Philips Medical Systems, Best, the Netherlands), with the RF body coil as transmitter and receiver.

2.1.1 uTE PROTOCOL

Figure 1 shows a schematic time sheet of the 3D "STEPS" uTE sequence that was used in this work, and the corresponding k-space readout trajectory. A short (48 μs) non selective RF block pulse is followed by a short phase encoding gradient. In the x- and z-directions the gradients are applied simultaneously to create a radial k-space readout trajectory. The sampling of the k-space data is also performed during the gradient ramp, before the gradient has reached its maximum value. The TE of the sequence is determined by the time gap between the end of the RF pulse and the beginning of the readout gradients. Thus, the shortest TE is limited by the ring down and tuning of the RF coil. Before preceeding RF pulse, the gradients are refocused in the x and z (readout) directions, and spoiled in the y (phase) direction.

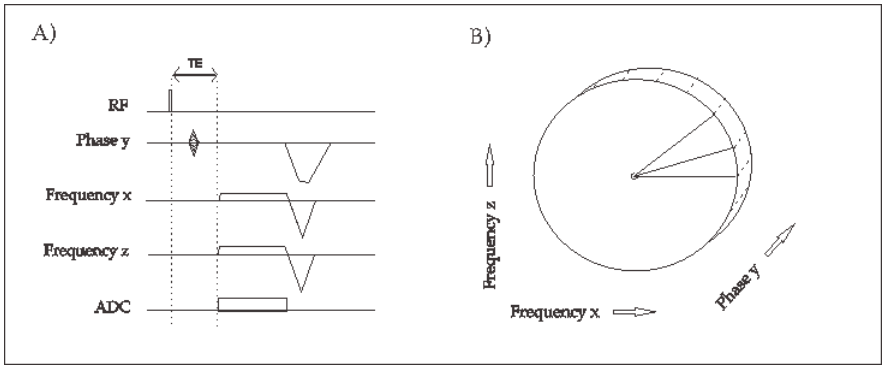

Figure 1: The pulse sequence (A) and the corresponding k-space readout trajectory (B) for the 3D "STEPS" uTE sequence.

In this work, a standard protocol was set up according to Figure 2. The standard protocol was used as a starting point for the MRI measurements. From this protocol, scan parameters that were expected to influence the signal behaviour were varied, i.e. TE (0.1 - 6 ms), field of view (450 - 500 mm), gradient mode ("maximum" and "enhanced", see Appendix A), voxel size (3x3x15 - 7x7x15 mm^3), pixel bandwidth (272 - 1083 Hz) and radial density (120 - 170%). In *in vivo* measurements, uTE images acquired with a "koosh-ball" trajectory were compared to images acquired with the "STEPS" trajectory of the standard protocol. The "koosh-ball" trajectory had radial read out in all three directions, which creates a sphere in k-space with isotropic voxels.

* Aquisition method: 3D radial, "STEPS"
* Echo time: 0.16 ms
* Repetition time: 3.6 ms
* Flip angle: 10^0
* Field of view: 500 mm (diameter)
* Voxel size: 5x5x15 mm^3
* Slice thickness: 15 mm
* Number of slices: 20
* Pixel bandwidth: 721 Hz
* Radial density: 170%
* Gradient mode: Maximum

Figure 2: The uTE standard protocol.

A comparison between the uTE sequence (using TE=0.64 ms) and a conventional asymmetric gradient echo (aGRE) sequence was performed. In the comparison, both sequences had the same settings for TE, repetition time (TR), flip angle, field of view (FOV), voxel size, pixel bandwidth (BW) and gradient mode. One measurement was also performed on a 3.0 T MR system (Philips Achieva, Philips Medical Systems, Best, the Netherlands), with purpouse to compare the phanom images to images acquired on the 1.5 T MR system. For the 3.0 T measurement, the parameter settings of the standard protocol were used, exept for the TR which was 10 ms. The RF body coil was used as transmitter and reciever.

2.1.2 PHANTOMS

To study the effect of the various scan parameters on the signal behaviour, two different phantoms were used. Phantom 1 consisted of a large PMMA volume (41x28x22 cm^3) with two compartments (Figure 3). The main compartment of the phantom was filled with $MnCl_2$ doped water with a concentration of 1.2 mmol/l (T_1=193.0 ms ± 0.6 ms, T_2=21.8 ms ± 0.2 ms). The smaller and liver shaped compartment (compartment 2) was filled with heavily NaCl doped water with a concentration of 1.2 mol/l. The T_1 and T_2 relaxation times of the NaCl doped water were not measurable with commersial MRI techniques.

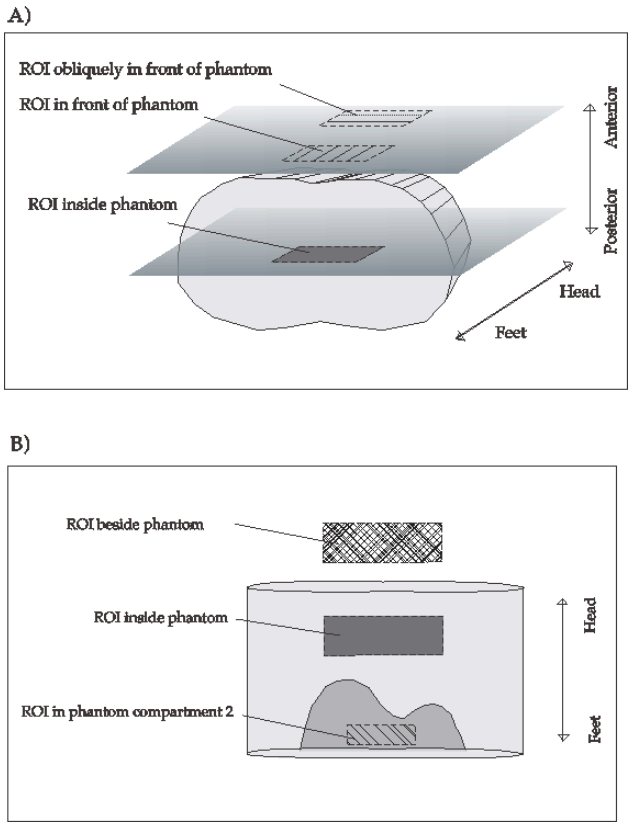

Figure 3: (A) Transversal and (B) coronal views of Phantom 1. The figure also shows image planes and regions of interest (ROI:s) used in the signal analysis.

To simulate respiratory motion, Phantom 1 was placed in a wooden frame. The frame was connected via a wooden lath to a pneumatic engine, which gave the phantom a head-feet motion of about 9 mm/s. There was only minor motion in the anterior-posterior direction, caused by vibrations and inevitable motion inside the liquid.

Phantom 2 mimicked a delta function in image space and consisted of a straw with a diameter smaller than the voxel size ($\varnothing$=3 mm). The straw was fixated in a rigid container and filled with the $MnCl_2$ doped water used in the main compartment of Phantom 1.

Before scanning, the phantoms were carefully positioned at the isocenter of the magnet. Phantom 2 was positioned with the straw parallell to the symmetry axis of the magnet and Phantom 1 was positioned as described by Figure 3.

2.1.3 SNR MEASUREMENTS

To determine the SNR of the phantom measurements, the electronic and thermal noise were measured with a dynamic noise scan method [9]. Each measurement consisted of two dynamic scans, where the first was a regular scan and the other was an acquisition without RF excitation and gradient encoding. At least 30 seconds passed between the scans for the signal from the first scan to subside. A measure of the SNR was obtained by dividing the mean signal in a ROI in an image from the first scan with the mean signal in the same ROI in an image from the second scan.

2.1.4 *IN VIVO* MEASUREMENTS

Three healthy volunteers participated in the *in vivo* measurements. The volunteers were placed with the lungs centered in the magnet. The width of their shoulders was smaller than the FOV (50 cm) in the right-left direction.

In the beginning of this work, *in vivo* uTE images were acquired with the standard protocol (Figure 2), using respiratory navigation. These images were later compared to images acquired with the optimized uTE sequence during free breathing. For the optimized uTE sequence, the parameter settings that differed from the standard protocol were voxel size (3x3x3 mm^3), BW (1083 Hz) and aquisition method ("koosh-ball"). Also, *in vivo* images acquired with the uTE sequence (using the standard protocol, exept TE=0.64 ms) were compared to images acquired with an aGRE sequence. In the comparison, both sequences had the same settings for TE, TR, flip angle, FOV, voxel size, BW and gradient mode. These images were acquired during breath hold.

2.2 SIGNAL ANALYSIS

All images were analysed in ImageJ, version 1.43u (open source software, National Institutes of Health, http://rsb.info.nih.gov/ij). The signal was analysed in image space and, for some of the measurements, in k-space. To enable comparison, the signal gain was fixed within each scan session.

In the images of Phantom 1, the mean signal was determined in ROI:s at different positions in the images (Figure 3). The ROI inside the phantom was placed in the main compartment. The ROI beside the phantom and the ROI in front of the phantom were positioned at approximately the same distance from the phantom. Both "true" and unwanted signal was studied in the images of Phantom 1. Generally, unwanted signal is called noise. In this work, the word noise will refer to the electronic and thermal noise. The unwanted signal from motion will be called motion disturbance and the effect on the signal due to the PSF of the MR acquisition will be called signal leakage.

The images of Phantom 2 were used to further investigate the signal behaviour of the uTE and aGRE sequencies. Signal profiles were acquired in the right-left

direction of a transversal image, and in the anterior-posterior direction through a stack of coronal images. The full-width-half-maximum (FWHM) of the signal profiles was used as a measure of the point-spread-function (PSF).

To study the signal behaviour in the *in vivo* images, ROI:s were placed in the upper part of the left lung (excluding major vessels from the ROI), in the muscle tissue of the right biceps and in the liver tissue (Figure 15).

2.3 MRI STATISTICS

All calculations and and statistic analysis were performed using Microsoft Excel 2008 for Mac.

To determine the precision in the measurements of Phantom 1, some measurements were repeated six times. The standard deviation was calculated and used as a measure of the variation. The standard deviations are displayed in the figures of Section 3. To determine if differences were significant, a Mann-Whitney test was performed. A 95% confidence was concidered statistically significant.

3 RESULTS

3.1 PHANTOM MEASUREMENTS

Results from the phantom measurements showed that several scan parameters affect the uTE signal, i.e. TE, BW, voxel size, radial density and gradient mode. The change in FOV did not affect the signal significantly. Also, the phantom itself influences the signal. For example, the signal behaviour was different if the phantom was moving or if it was at rest.

The signal levels in different parts of a uTE image of Phantom 1 are shown in Figure 4. The signal inside the phantom was much higher than outside the phantom (13-1300 times higher depending on the position of the ROI). The signal outside the phantom was largest in front of the phantom, i.e. in the slice encoding direction. The signal obliquely in front of the phantom was so low that it is hardly visible in the chart. The signal in front of the phantom was about five times higher than the signal beside the phantom and followed in general the signal level inside the phantom.

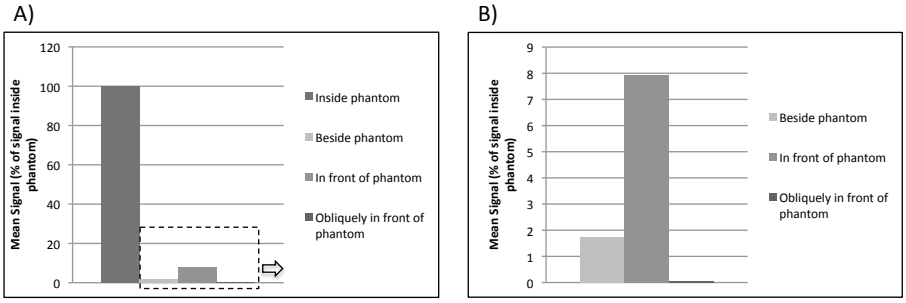

Figure 4: (A) Signal levels in different parts of the image for the standard uTE scan protocol and (B) a zoomed chart of the signal levels outside the phantom.

The signal at the position beside Phantom 1 showed a similar spatial varia-

tion as the sum of the signal inside both compartments of the phantom (Figure 5).

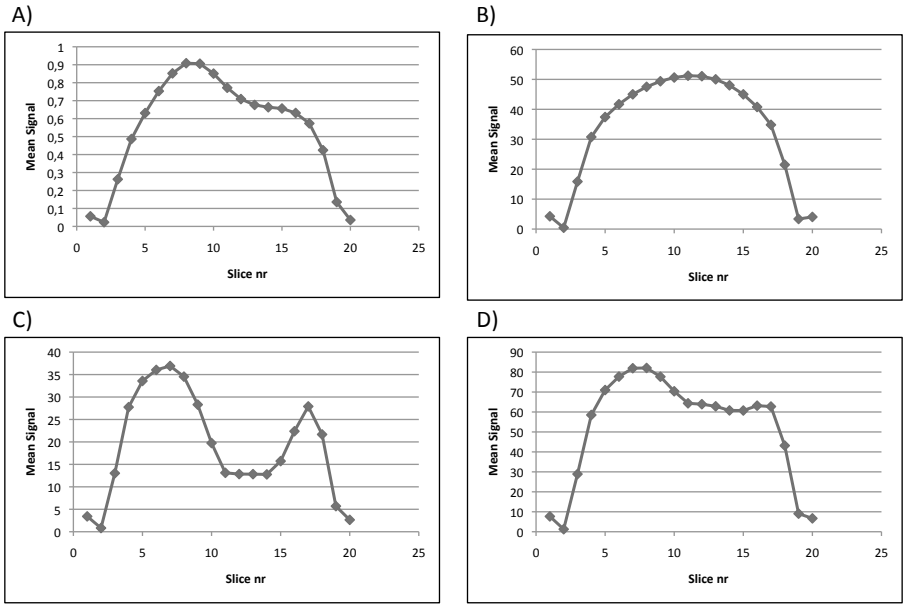

Figure 5: Spatial variation in the slice encoding (anterior-posterior) direction of mean signal in ROI:s at different positions - (A) beside phantom, (B) inside phantom (main compartment), (C) inside phantom compartment 2 and (D) sum of signal in both compartments of the phantom.

The signal inside Phantom 1 decreased with increased TE (Figure 6). Assuming an exponential relaxation, the T2* relaxation time of the liquid used in the main compartment was 16.9 ms. The signal outside the phantom also increased with decreased TE.

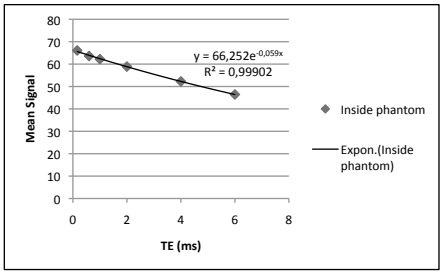

Figure 6: Signal inside Phantom 1 for different TE. An exponential regression function is inserted in the chart.

When the BW increased, the signal inside Phantom 1 decreased (Figure 7a). The signal beside the phantom was also influenced by the BW, but in a non linear manner. A BW of 542 Hz gave the lowest signal beside the phantom (Figure 7b).

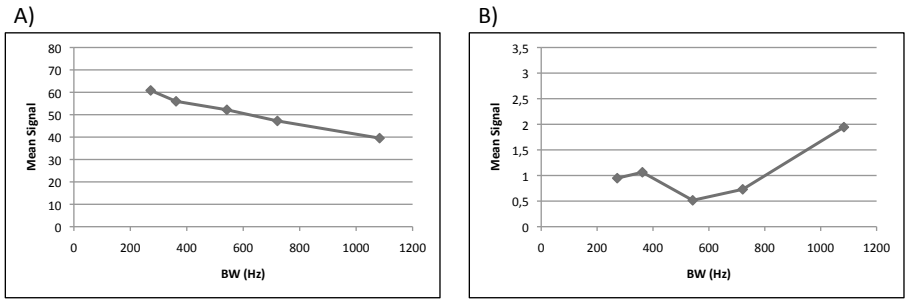

Figure 7: Signal (A) inside Phantom 1 and (B) beside Phantom 1 for different BW.

When the voxel size increased, the signal inside Phantom 1 increased (Figure 8a). The signal beside the phantom showed the opposite behaviour and decreased when the voxel size increased (Figure 8b).

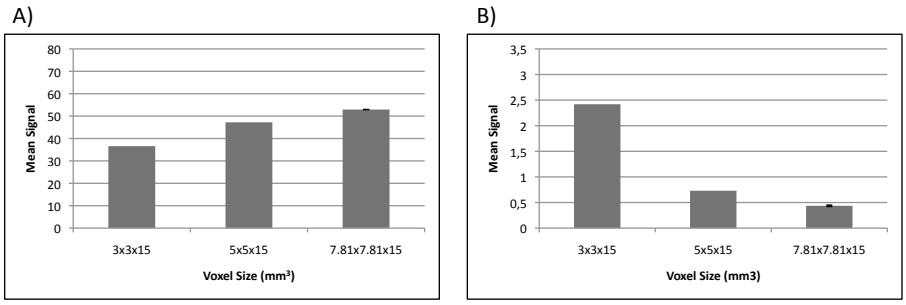

Figure 8: Signal (A) inside Phantom 1 and (B) beside Phantom 1 for different voxel size.

When the gradient mode was changed from "maximum" to "enhanced", the signal inside Phantom 1 decreased and the signal beside Phantom 1 increased (Figure 9). Also, the precision of the measurements was reduced after changing the gradient mode from "maximum" to "enhanced".

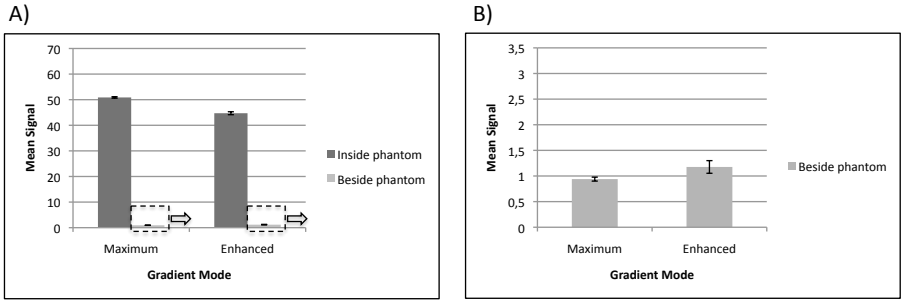

Figure 9: Signal (A) inside Phantom 1 and (B) beside Phantom 1 for different gradient mode, see Appendix A.

When the radial density was decreased from 170 to 120%, the signal inside Phantom 1 was slightly decreased. The change in signal was significant, but small (from 46.94 to 46,87, i.e. 0.2% difference).

The lowest TE achievable was 0.16 ms for the uTE sequence and 0.64 ms for the aGRE sequence. uTE images acquired with the longer TE (0.64 ms) showed a different signal behaviour than the corresponding aGRE images. The signal

inside Phantom 1 was significantly higher (∼5%) in the aGRE images than in the uTE images (Figure 10a). Outside Phantom 1 the signal was lower (about 5-25 times) in the aGRE images than in the uTE images (Figure 10b). In the uTE images, the signal increased close to the edges of the anterior-posterior FOV (Figure 11) resulting in the much higher signal in front of the phantom in the uTE images than in the aGRE images (Figure 10b). Also, the uTE signal profile over the anterior-posterior FOV showed a more narrow shape of the phantom (Figure 11).

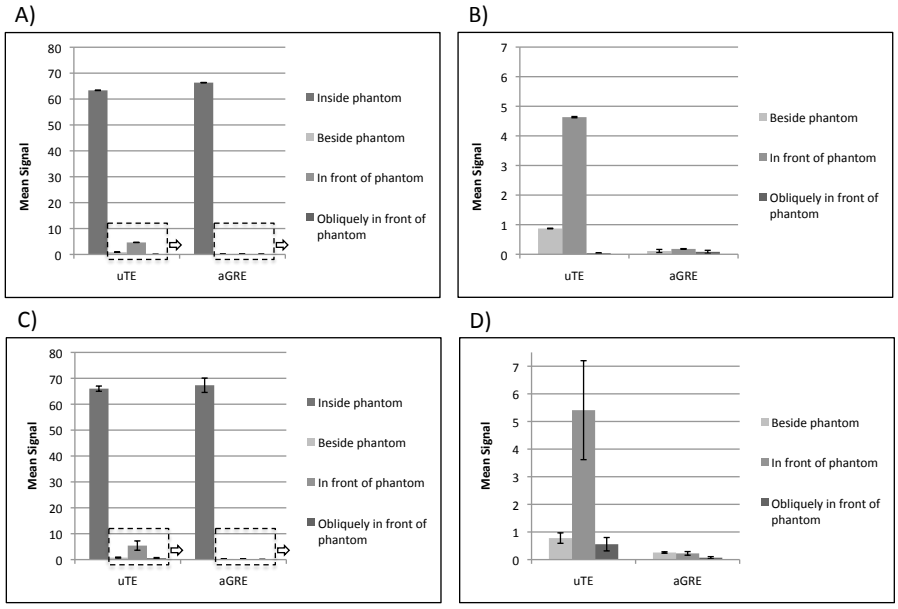

Figure 10: Signal in uTE and aGRE images of (A) Phantom 1 at rest and (C) Phantom 1 in motion. Zoomed charts of the signal levels (B) outside Phantom 1 at rest and (D) outside Phantom 1 in motion.

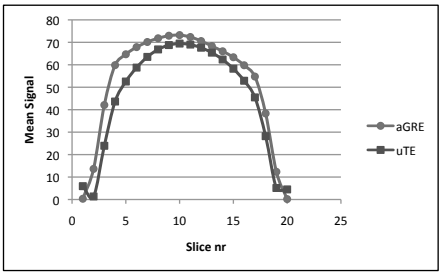

Figure 11: Signal profiles in the slice encoding (anterior-posterior) direction in aGRE and uTE images of Phantom 1.

The effect of motion was different in the uTE and the aGRE images (Figure 12). In the aGRE images, motion created traditional ghosting in the phase encoding direction. In the uTE images, motion caused blurring all over the image and the visibility was less affected than in the aGRE images. When Phantom 1 was moving, the aGRE measurements gave signal levels with larger variation inside the phantom (Figure 10c).

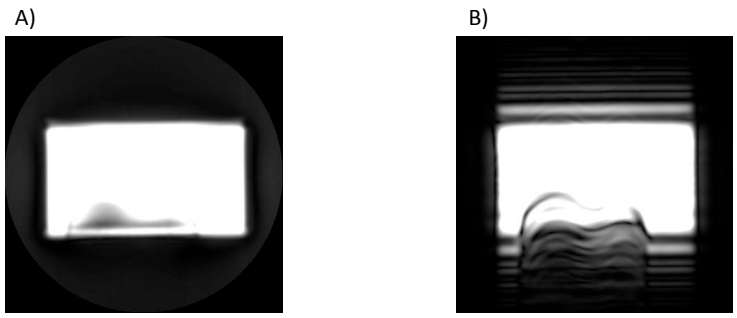

Figure 12: The effect of motion in (A) a uTE and (B) an aGRE image of Phantom 1.

Imaging performed on Phantom 1 showed that Phantom 1 was not suitable for uTE studies in 3.0 T MR systems, as it gave severe dielectric signal artefacts (Figure 13). Therefore, no further 3.0 T measurements were performed.

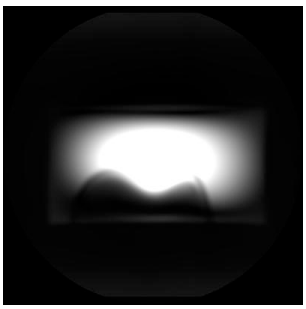

Figure 13: uTE image of Phantom 1, aquired on a 3.0 T MR system, TE=0.16 ms, TR=10 ms.

The noise level, measured on Phantom 1 with the dynamic scan method (Section 2.1.3), was very low compared to the total signal level. For the standard uTE sequence, the signal level inside the phantom was 50.2 (standard deviation 3.7), while the noise level was $6.0*10^{-4}$ (standard deviation $4.6*10^{-3}$). The low noise value created discretization errors in the SNR.

The measurements performed on Phantom 2 showed that the width of the PSF was of the same order for the aGRE sequence as for the uTE sequence. The FWHM was 5.7 mm for aGRE and 6.1 mm for uTE in the right-left direction. In the anterior-posterior direction, i.e. in the slice encoding direction, the FWHM was 33.2 mm and 32.7 mm, respectively. For a radial density of 4%, the k-space data corresponding to transversal uTE images of Phantom 2 showed a non constant signal level, where the signal decreased towards the k-space center (Figure 14).

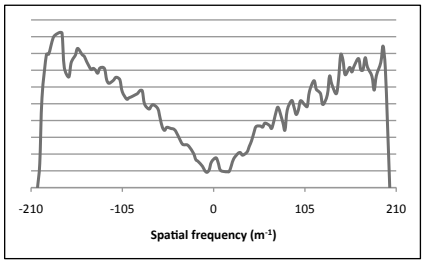

Figure 14: A signal profile along the (k_x,0) axis, corresponding to a transversal uTE image of Phantom 2, aquired with a radial density of 4%.

3.2 *IN VIVO* MEASUREMENTS

The *in vivo* measurements showed about 18% lower signal in lung in an aGRE image than in an image acquired with the corresponding uTE sequence (Figure 15). The signal in muscle was about 17% higher in the aGRE image.

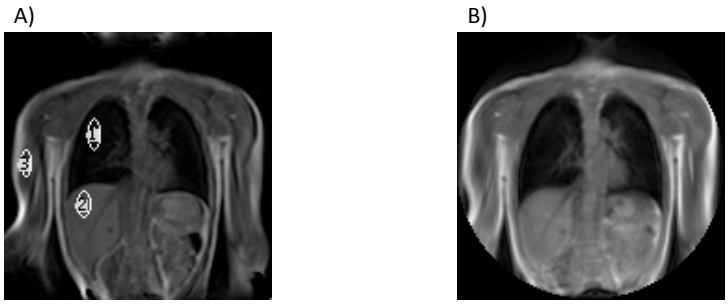

Figure 15: *In vivo* (A) aGRE and (B) uTE images of lung. The images were acquired during breath hold and the sequences had the same parameter settings for TE, TR, flip angle, FOV, voxel size, pixel bandwidth and gradient mode. (A) also shows the ROI:s used in the *in vivo* signal analysis.

For the uTE "STEPS" sequence, the signal in lung and in liver increased when the TE decreased from 0.64 ms to 0.16 ms. The signal in muscle though decreased when the TE decreased (Figure 16a). When the uTE images were

acquired with the "koosh-ball" technique, the signal showed a more theoretically expected dependence on TE, i.e. the signal increased also in muscle when the TE decreased (Figure 16b).

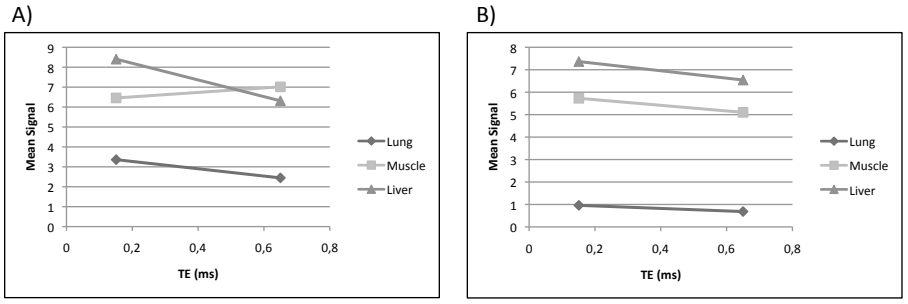

Figure 16: Signal in lung, muscle and liver in healty volunteer for two different TE values, using acquisition methods (A) uTE "STEPS" and (B) uTE "koosh-ball".

Optimizing the uTE protocol according to phantom experiences and previous knowledge, gave *in vivo* images of high quality. The overall visability and resolution was improved (Figure 17).

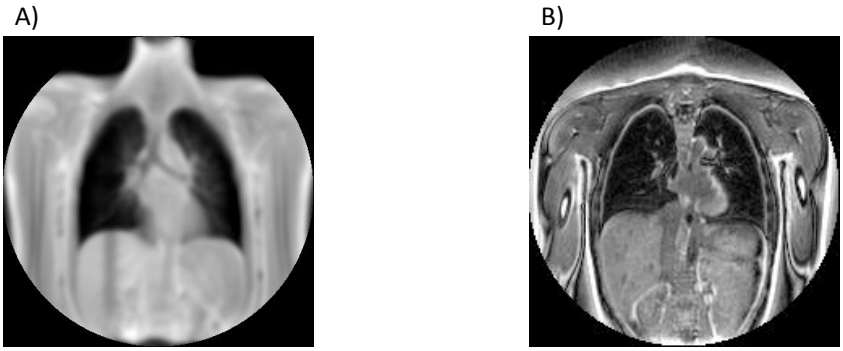

Figure 17: *In vivo* uTE images of lung (A) before and (B) after optimization of the uTE protocol. The scan parameters in (B) that differed from the standard protocol were voxel size (3x3x3 mm^3), BW (1083 Hz) and aquisition method ("koosh-ball"). (A) was acquired with respiratory navigation and (B) was acquired during free breathing.

4 DISCUSSION

Lung imaging is challenging due to low SNR and cardiac and respiratory motion. A sequence that has showed promising results for lung imaging is the uTE sequence [5] [6]. In this work, we have, with use of different phantoms, showed that the uTE signal depends on the imaged object, e.g. its motion and geometry, and on several scan parameters. Based on the knowledge of the signal behaviour from the phantom measurements, and via well-established theoretical associations, the scan protocol used for uTE imaging was optimized and the quality of the lung imaging was improved (Figure 17). Additional optimization may improve the image quality even further.

To remove confounding effects of physiological variation and because human lung does not provide enough signal for studies of the signal behaviour, two different phantoms were used in the measurements. Phantom 1 was used to study the signal behaviour - including noise, motion disturbance and signal leakage - in a true sized object. Phantom 2 mimicked a delta function, which facilitated closer studies of the signal behaviour in both image space and k-space. Imaging was performed solely on a 1.5 T MR system, since the images acquired on a 3.0 T MR system showed severe dielectric artefacts (Figure 13).

The SNR measurements, performed on Phantom 1 with a dynamic scan method (Section 2.1.3), showed that the noise in the images was neglible - $6.0*10^{-4}$ compared to a signal inside the phantom of 50.2. Therefore, none of the changes in signal in the images of Phantom 1 are results of change in noise level, not even beside or in front of the phantom. Instead, there are other phenomena that effect the images much more.

The signal inside Phantom 1 was expected to decrease exponentially with increased TE. The exponential regression of Figure 6 gave a measure of the T_2* relaxation time of the $MnCl_2$ doped water of 16.9 ms. This is a reasonable result

as the T_2 relaxation time of the liquid was 21.8 ms. Thus, the results for the signal behaviour of the uTE sequnece regarding TE does not differ from what is theoretically expected.

When the voxel size was increased, the signal in the images was expected to increase linearly. The signal inside Phantom 1 followed this expected result (Figure 8a). Beside the phantom the signal instead decreased with increased voxel size (Figure 8b). The smallest voxel size - 3x3x15 mm^3 - gave the highest signal beside the phantom. This was probably due to Nyquist streakings [3], which became more severe when the size of k-spece increased, i.e. when the voxel size decreased. The radial density, the FOV and the voxel size all affect the sampling density and hence the fulfilment of the Nyquist theorem. Certain combinations of these parameters result in undersampling of high spatial frequency signal. Therefor, the settings for these three parameters must be concidered in relation to each other. For example, the FOV used in the *in vivo* measurements gave undersampling of the higher spatial frequencies, even for the highest radial density possible (170%). However, when the FOV was decreased from 500 mm to 450 mm, there was no significant change in signal. The change should probably have been bigger for the signal from the Nyquist streakings to be affected significantly.

The voxel size also influences the PSF. The signal profile in a uTE image of Phantom 2 showed a FWHM of 5.7 m in the right-left direction, where the voxel width was 5 mm. In the anterior-posterior direction, where the voxel width was 15 mm, the FWHM was 33.2 mm. The latter value exceeds what is theoretically expected, and the reason is probably the small reconstruction matrix (20) in this direction (slice direction). The PSF gives rise to signal leakage which can be severe in *in vivo* images. As expected, the signal outside Phantom 1 in an image acquired with the standard protocol substantially consisted of signal leakage. This was shown in the anterior-posterior signal profiles in different parts of uTE images of Phantom 1 (Figure 11). The spatial variation of

the signal beside the phantom correlated to the spatial variation of the sum of the signal in both compartments of the phantom, which indicates signal leakage.

The T_2* relaxation time of the $MnCl_2$ doped water in Phantom 1 (16.9 ms) was too long for the signal to significantly decrease during the acquisition. Therefor, the BW - which is inversely prportional to the acquisition time - should not influence the signal inside Phantom 1. Results show, however, that the signal inside Phantom 1 decreased when the BW increased. Since the size of k-space was constant during these measurements, the signal increase could be an effect of change in gradient strength. Changing the gradient strength will change the conditions for the eddy current and ramp sampling compensations. As a result, the effect of these compensations might detoriate and cause a signal decrease.

The signal dependence on gradient strength and gradient ramp was also showed when the gradient mode was changed from "maximum" to "enhanced" (Figure 9). It seems as the eddy current and gradient ramp compensations, as currently implemented, have optimal settings for a certain BW and gradient mode. These optimal settings should be used when the compensations are not adaptable to different parameter settings. Results show that the optimal BW, if the T2* relaxation during acquisition is not taken into consideration, is 542 Hz (Figure 7).

The signal increased slightly with increased radial density. Increasing the radial density will increase the oversampling of data in the k-space center. Before image reconstruction, this oversampled data needs to be density weighted to display the object correctly [2]. Measurements performed on Phantom 2 with a radial density of 4% show the effect of such weighting function (Figure 14). The deviation from the theoretically expected result of a constant function in k-space also shows that the density weighing function, as it is currently implemented, has an optimal value for a certain radial density. This optimal value should be used when the weighting function is not adaptable to different param-

eter settings. If undersampling of high frequency data cannot be avoided, the weighting function needs to compensate for this as well. The density function could weight down the influence of the high spatial frequencies, given that less well defined edges are acceptable.

A comparison between the uTE sequence and an aGRE sequence was performed. The purpose was to use the conventional aGRE sequence as a tool to compare the signal and artifact behaviour of the uTE sequence to something well-known. The sequences showed differences in signal behaviour and in the signal distribution over the imaged region. For the uTE sequence, the signal was significantly lower inside Phantom 1 (Figure 10a, 11) and significantly higher outside the phantom (Figure 10b). Even though the sequences had the same parameter settings for TE, TR, flip angle, FOV, voxel size, pixel bandwidth and gradient mode, it is not evident for the signal levels to be the same for the two sequences. The signal in the uTE images is affected by the density weighting, where the radial density chosen is not assuredly optimal, and by undersampling in the angular direction. The asymmetry of the aGRE sequnece also makes it non trivial to compare the signal levels. This is also the case for the comparison between the signal levels in different parts of the *in vivo* uTE and aGRE images (Figure 15).

It is interesting to note that the signal profile over Phantom 1 in the uTE image was more narrow than in the aGRE image, and displayed an increase at the edges of the imaged region (Figure 11). This increase is not due to a higher signal leakage for the uTE sequence, since the FWHM of signal profiles over Phantom 2 were of the same size in uTE and aGRE images. Thus, the reason for the discrepancy between the signal profiles are yet unknown. Further understanding of the uTE regridding and density weighting process might give an idea of the reason for this result.

An important difference between the aGRE and uTE sequences, is the difference

in motion sensitivity. As a result of the evenly distributed motion artefact of the uTE sequence, the uTE images of Phantom 1 in motion was less affected by the motion (Figure 12). The uTE signal was also less dependent on the spatial position of the phantom, since the scan time was longer compared to the time frame of the motion. As a result, the variation in signal for repeated measurements on Phanom 1 in motion was lower for the uTE sequence.

Because of the motion insensitivity of the uTE sequence, it is possible to perform uTE imaging during free breathing. This is beneficial for patients as the scan times will be shorter when free breathing is used instead of navigation and gating methods. It is also important to avoid scan protocols with breath hold, which can be streneuous especially for patients with lung dysfunction. If performed during free breathing, *in vivo* uTE imaging of lung should be performed with "koosh-ball" uTE, especially when the images are coronal. It is unadvantageous if the direction of respiratory motion coincides whith the phase encoding direction. It is therefore advantageous that the "koosh-ball" trajectory is without phase encoding. Consequently, this work shows better, more theoretically reasonable results for the signal behaviour in uTE "koosh-ball" *in vivo* images than in uTE "STEPS" *in vivo* images (Figure 16).

After the optimization of the uTE sequence, the parameters that were changed compared to the standard protocol were voxel size (3x3x3 mm^3), BW (1083 Hz) and aquisition method ("koosh-ball"). The small voxel size was chosen because it decreased the signal leakage, which would leak signal into the lung from surrounding tissues. A small voxel size, however, increased the Nyquist streakings, but the relativelly even distribution of this artefact was concidered less severe. In the measurements of Phantom 1, the optimal BW seemed to be 542 Hz. For the T_2* relaxation time of lung (about 1 ms), however, the acquisition time is crucial. Therefore, the results from the phantom measurements were set aside for the benefit of the well-established association between acquisition time and T_2* signal decay.

The question is - is uTE a suitable sequence for MR lung imaging? Yes, the results are promising. The quality of the lung images has improved during this work, but further optimization and *in vivo* measurements are needed. Further optimization of the uTE sequence aims at maximizing the signal from lung parenchyma. Then, it is important to ensure that the signal really originates from lung parenchyma, considering the non trivial artifact behaviour of the uTE sequence. When a high enough signal from lung parenchyma is acquired, it is possible to use and manipulate the signal with conventional methods to receive different functional contrasts. The uTE sequence will thereby have the potential to be used in the diagnostics of lung diseases, e.g. COPD, asthma and ILD.

In conclusion, this work elucidated the signal behaviour of the uTE sequence. The uTE signal increased with increased radial density and voxel size, and with decreased TE and BW. The results mostly followed the theoretically expected associations. Comparisons showed differences in signal behaviour between the uTE sequence and a corresponding aGRE sequence. Some of these differences are still to be fully explained. The quality of *in vivo* lung MR images was improved after optimization of the uTE scan protocol. Further understanding of the uTE regridding and density weighting process is needed to continue the optimization process.

A GRADIENT MODE SPECIFICATIONS

- Maximum - The maximum gradient strength and slew rate are used.
- Enhanced - The setting "enhanced" supports the dual mode gradients. The system will operate with a double gradient amplitude at half the slew rate with respect to the regular gradients in order to comply with international safety standard.

B CONTACT INFORMATION

Author:
Katrin Johansson
Department of radiation physics
University of Gothenburg
phone: +46 709 619988
mail: katrinjohansson@hotmail.com

Supervisor:
Kerstin Lagerstrand, Ph.D.
Medical physicist
Sahlgrenska University Hospital
MR centre
phone: +46 31 3435277
mail: kerstin.lagerstrand@vgregion.se

References

[1] P D Gatehouse *et al.* Magnetic resonance imaging of short t2 components in tissue. *Clinical radiology*, 58:1–19, 2003.

[2] J G Pipe *et al.* Reconstructing mr images from undersampled data: Data-weighting considerations. *Magnetic Resonance in Medicine*, 43:867–875, 2000.

[3] K Scheffler *et al.* Reduced circular field-of-view imaging. *Magnetic Resonance in Medicine*, 40:474–480, 1998.

[4] A C S Brau *et al.* Cine magnetic resonance microscopy of the rat heart using cardiorespiratory-synchronous projection reconstruction. *Journal of magnetic resonance imaging*, 20:31–38, 2004.

[5] J Zapp *et al.* Proton mri of human lung using 2d radial acquisition at 1.5 t and 3.0 t. ISMRM#2510, 2010.

[6] Y Ohno *et al.* Lung mr imaging with ultra-short te at 3.0t system: Capability for pulmonary functional loss due to copd. ISMRM#203, 2010.

[7] M Takahashi *et al.* Ultra-short echo time (ute) mr imaging of the lung: comparison between normal and emphysematous lungs in mutant mice. *Journal of magnetic resonance imaging*, 32:326–33, 2010.

[8] M Zurek *et al.* Validation of simple and robust protocols for high-resolution lung proton mri in mice. *Magnetic Resonance in Medicine*, 64:401–407, 2010.

[9] P Kellman *et al.* Image reconstruction in snr units: A general method for snr measurement. *Magnetic Resonance in Medicine*, 54:1439–1447, 2005.